LASER & PHOTONICS REVIEWS
www.lpr-journal.org

Nonlocal Metasurfaces-Enabled Analog Light Localization for Imaging and Lithography

Minkyung Kim, Dasol Lee,* Jaekyung Kim, and Junsuk Rho*

Localization of light spots in a given image is a common task in digital processing but is challenging in analog. Herein, a periodic nonlocal metasurface that has an optical transfer function defined in reciprocal space is proposed to resolve this issue. Assuming an ideal optical transfer function that encodes that of a local lens, the selective spot size reduction of incident Gaussian beams and sharpening of a patterned incidence with a Gaussian line shape are demonstrated. A realistic nonlocal metasurface comprising a trilayer structure with air grating on top that operates as a 2D analog light localizer under unpolarized incidence is presented. Nonlocal metasurfaces, combined with conventional optics, are expected to improve the resolution by sharpening the spatial features and find applications in diverse scientific fields such as medical, materials, and life science.

1. Introduction

Optics permeates our everyday existence and is at the forefront of scientific exploration. One important component that is indispensable in most optical systems is the lens. The underpinning of lenses is the locality in that the illuminated light interacts locally and pointwise with each spatial point of the lenses. To tailor the wavefront and accordingly the flow of light, refractive lenses with geometric curvatures[1] and artificially engineered materials called metasurfaces comprising spatially varying unit structures[2–13] have been developed. These local lenses have an optical transfer function (OTF) defined in real space and thus can be understood as multiplication operators in real space.

Alternatively, one may design a periodic metasurface with strong nonlocality, i.e., a nonlocal metasurface,[14,15] to focus light as the local lens but in a wavevector (**k**) space. Because of translational symmetry, the nonlocal metasurface has an OTF defined purely in the **k** space[16] and corresponds to a multiplication operator in the **k** space rather than in real space. Therefore, in contrast to a local lens that uniformly magnifies or demagnifies all the spatial features of an input image, including the spot size and spatial positions, a nonlocal metasurface cannot alter the spatial position of the generated beams, leading to selective control of the size of the light spot while preserving other spatial information. Furthermore, nonlocality-based imaging mitigates spatial image distortions originating from misalignment between the lens center and image. However, despite these advantages and potential applications, a nonlocal metasurface with such functionalities remains unexplored.

This paper presents nonlocal metasurfaces that act as 2D analog light localizers under unpolarized incidence. We first demonstrate that a nonlocal metasurface with an ideal OTF selectively reduces the spot sizes of incident Gaussian beams while maintaining their initial positions intact. The localization effect of the nonlocal metasurface not only occurs under an ideal Gaussian beam, but also can be found under a patterned incidence with a smooth line shape. Finally, we propose a realistic nonlocal metasurface with a trilayer structure, the top of which has a diffractive air grating in a square lattice, and investigate its applicability in imaging and lithography. The nonlocal metasurface sharpens the spatial features of the incidence at the speed of light without requiring digital image processing, thereby enhancing the resolution of a given system. Analog light localization empowered by nonlocal metasurfaces has widespread applications in various fields that involve imaging and light illumination.

M. Kim
School of Mechanical Engineering
Gwangju Institute of Science and Technology (GIST)
Gwangju 61005, Republic of Korea
E-mail: m.kim@gist.ac.kr

D. Lee
Department of Biomedical Engineering
Yonsei University
Wonju 26493, Republic of Korea
E-mail: dasol@yonsei.ac.kr

J. Kim, J. Rho
Department of Mechanical Engineering
Pohang University of Science and Technology (POSTECH)
Pohang 37673, Republic of Korea

J. Rho
Department of Chemical Engineering
Pohang University of Science and Technology (POSTECH)
Pohang 37673, Republic of Korea

J. Rho
POSCO-POSTECH-RIST Convergence Research Center for Flat Optics and Metaphotonics
Pohang 37673, Republic of Korea

The ORCID identification number(s) for the author(s) of this article can be found under https://doi.org/10.1002/lpor.202300718

DOI: 10.1002/lpor.202300718

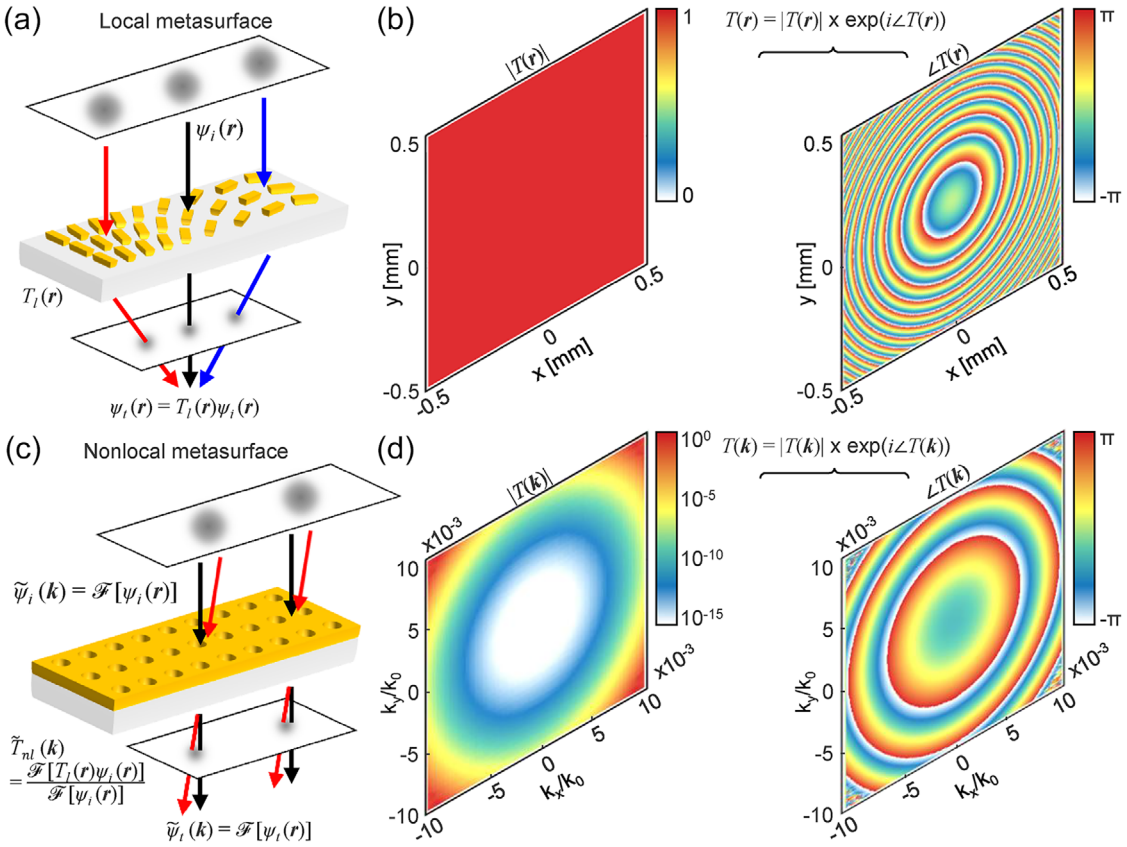

Figure 1. Principle of a nonlocal metasurface for light localization. a) Schematic of a local metalens and its spatial nonuniformity and locality. b) Unity amplitude and quadratic phase profiles of the optical transfer function (OTF) in real space. c) Schematic of a nonlocal metasurface and its spatial uniformity and nonlocality. d) Amplitude and phase profiles of the OTF in the **k** space.

2. Results and Discussion

2.1. Principle

First, we briefly revisit focusing using local lenses and compare it with nonlocality-based focusing. Consider a coordinate system whose origin lies at the lens center and let z be the direction of propagation. The beam transmitted through the local lens follows (**Figure 1a**)

$$\psi_t(\mathbf{r}) = T_l(\mathbf{r})\psi_i(\mathbf{r}) \tag{1}$$

where ψ is the electric field, the subscripts i and t represent the incident and transmitted beams, respectively, $T_l(\mathbf{r}) = \exp\left[-ik_0(\sqrt{x^2+y^2+f^2}-f)\right]$ is the OTF of the lens (Figure 1b), $\mathbf{r} = (x, y)$ is the lateral spatial coordinates of the lens, k_0 is the free space wavenumber, and f is the focal length. When f is much larger than the lateral dimension of the lens ($x^2 + y^2 \ll 4f^2$), it has a quadratic phase profile and converts the incident Gaussian into another Gaussian that has a Rayleigh length of $z_R' = z_R/(1 + z_R^2/f^2)$ where z_R is the Rayleigh length of the incidence. It can be demonstrated that after propagating through free space by a distance of $z_p \ll fz_R/(f + z_R)$, the incident Gaussian centered at $\mathbf{r}_0$ is converted to a Gaussian that is centered at $\mathbf{r}_0'$ and has a beam radius of w', where

$$\mathbf{r}_0' = (1 - \frac{z_p}{f})\mathbf{r}_0$$

$$w' = (1 - \frac{z_p}{f})w_0 \tag{2}$$

and w_0 denotes the incident beam waist. This uniform rescaling holds with a slightly modified ratio when the previous assumption ($z_p \ll fz_R/(f + z_R)$) is invalid. A detailed analysis, including the derivation, can be found in the Section S1 (Supporting Information). Equation (2) implies that the local lens reduces not only the beam radius by $1 - z_p/f$ but also every piece of spatial information the incidence contains, including the feature size and position, by the same ratio. This uniform rescaling of an input image is an imperative aspect of optics, but cannot provide a selective localization of the spatial features.

The lack of such analog light localization can be overcome using recently attracted nonlocal metasurfaces.[14,15] We consider an ideal nonlocal metasurface that provides the same functionality as local lenses when the incidence is a Gaussian aligned at the lens center (Figure 1c). To obtain such a nonlocal metasurface, we encode the OTF of the local lens in the **k** space by dividing the Fourier transform of the transmitted beam by that of the incidence, as follows:

$$\begin{aligned}\tilde{T}_{nl}(\mathbf{k}) &= \tilde{\psi}_t(\mathbf{k})/\tilde{\psi}_i(\mathbf{k}) \\ &= \mathcal{F}[T_l(\mathbf{r})\psi_i(\mathbf{r})]/\mathcal{F}[\psi_i(\mathbf{r})]\end{aligned} \tag{3}$$

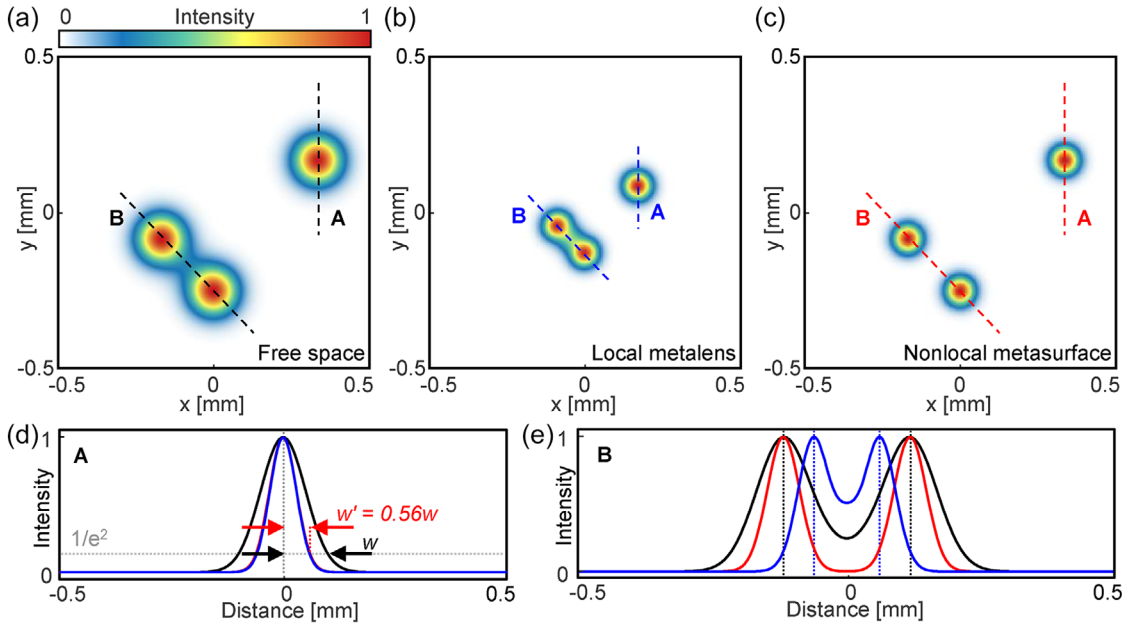

Figure 2. Imaging applications of the nonlocal metasurface compared to the local metalens. a–c) Intensity profiles of beams propagated through (a) free space, (b) local metalens, and (c) nonlocal metasurface when the incidence consists of multiple Gaussian beams. The wavelength and beam waist of all beams are 632.8 nm and 100 μm, respectively. The propagation distance from the nonlocal metasurface and focal length of the local metalens are both 30 mm. The intensity profile in (b) is shown at 0.49f apart from the metalens. d, e) Cross-sectional intensity profiles along the dashed lines A and B in (a–c). Black: free space, blue: local metalens, red: nonlocal metasurface. Blue and red curves in (d) are overlapped. All intensities are normalized to have a maximum value of unity.

where $\mathscr{F}$ denotes the Fourier transform operation, tilde indicates that the quantity is defined in the $\mathbf{k}$ space, ψ_i is an incident Gaussian centered at the origin, and ψ_t is the beam transmitted through the local lens obtained by Equation (1). The resultant OTF exhibits a strong incident angle dependence with a negligible amplitude at $\mathbf{k} = 0$ and a diverging feature that broadens the field profile in the $\mathbf{k}$ space (Figure 1d). For simplicity, we do not specify any polarization and assume that the OTF is polarization-independent.

The virtue of the nonlocal metasurface appears when the incidence is not aligned with the lens center. Because the OTF of the nonlocal metasurface is defined in the $\mathbf{k}$-space (Equation (3)) and spatial operations, such as translations in the xy plane, cannot affect the $\mathbf{k}$ space multiplication, the center positions of the incident and generated beams cannot differ. Thus, for an incident Gaussian that is centered at $\mathbf{r}_0 = (x_0, y_0)$, the transmitted beam also has its center at $\mathbf{r}_0$, regardless of the propagation distance from the lens. Meanwhile, diverging OTF (Figure 1d) broadens the $\mathbf{k}$ space profiles, resulting in the localization of the light spot by the same ratio as the local lens (Figure 1c). The proof can be found in the Section S1 (Supporting Information). Therefore, the nonlocal metasurface compresses each individual beam without changing its initial position. In this sense, the nonlocal metasurface operates as a light localizer. It is a stark contrast to the locality-based focusing (Equation (2)), where the beam center approaches the lens center as the beam propagates toward the focal point and hence the entire image is demagnified uniformly. Nevertheless, using nonlocal optics to selectively reduce the light spot size or to sharpen spatial features without destroying other information has not been attempted before.

The analog localization of light may also be achieved by constructing an optical setup to filter low $\mathbf{k}$ components in a narrow $\mathbf{k}$ space regime[17] (Section S2, Supporting Information) but this nonlocal metasurface provides the same effect in a few micrometer-scale thickness, reducing the form factor by several orders of magnitude. The nonlocal metasurface as a light localizer should be distinguished from recently reported spaceplates or space compressors[18–23] in that the nonlocal metasurface compresses the incident Gaussian regardless of its converging or diverging characteristics (see Section S3, Supporting Information for details).

2.2. Imaging Applications

A straightforward application of nonlocal metasurface is in imaging. For quantitative analysis, we define the localization ratio as w'/w, where w' is the radius of the beam transmitted through the metasurface and then propagating in free space by z_p and w is the radius without the metasurface. Here, the beam radius is defined as the distance from the center at which the intensity decreases to $1/e^2$. We simulate the propagation of multiple Gaussian beams that have a wavelength $\lambda = 632.8$ nm and beam waist $w_0 = 100\mu$m (**Figure** 2a) and pass through the local metalens (Figure 2b) and nonlocal metasurface (Figure 2c), respectively. The local metalens has a focal length of 30 mm. The OTF of the nonlocal metasurface is selected to serve the same function as that of the local metalens under a Gaussian beam with $w_0 = 100\mu$m centered at the origin using Equation (3). Note that the OTF diverges rapidly within $|\mathbf{k}| \leq 0.01k_0$ and the OTF

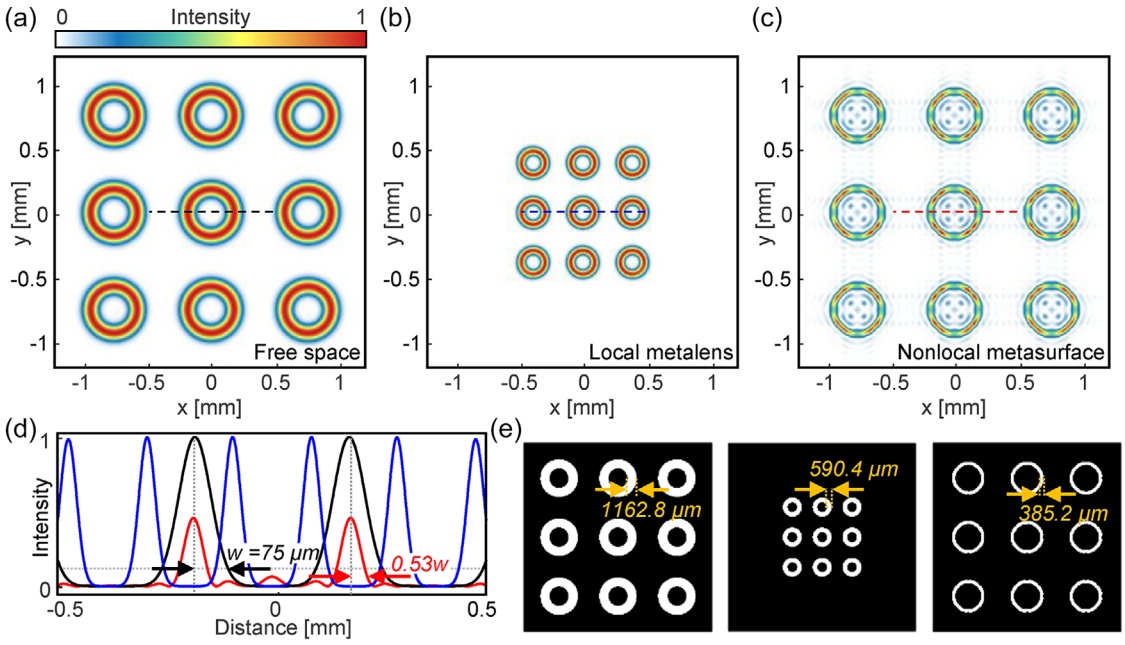

Figure 3. Lithography applications of the nonlocal metasurface compared to the local metalens. a–c) Intensity profiles of beams propagated through (a) free space, (b) local metalens, and (c) nonlocal metasurface when the incidence consists of multiple doughnut-shaped beams. The half-line width of the doughnut shape is 75 μm. The propagation distance from the nonlocal metasurface and the focal length of the local metalens are both 1 mm. The intensity profile in (b) is shown at 0.49f apart from the metalens. d) Cross-sectional intensity profiles along the dashed line in (a–c). Black: free space, blue: local metalens, red: nonlocal metasurface. e) Binary images of (a–c) when the threshold value is 0.3. Black and white denote unpatterned and patterned areas, respectively. All intensities are normalized to have a maximum value of unity.

at $|\mathbf{k}| > 0.01k_0$ is set to zero to prevent divergence as the $\mathbf{k}$ space profile of the incidence is negligible in this regime (See Section S1 and Figure S2, Supporting Information).

For $z_p = 0.49f$, the local metalens squeezes the incidence uniformly by a ratio of 0.56 (Figure 2b, also see Equation (S8) and Figure S1, Supporting Information for details). In contrast, the nonlocal metasurface reduces only the spot size of the beams by the same ratio and preserves their initial positions (Figure 2c). The difference between the local and nonlocal operations is indicated more definitely in the cross-sectional profiles (Figure 2d,e). Local metalens and nonlocal metasurface operate the same manner under a single Gaussian (Figure 2d), but they result in distinct images when two Gaussians partially overlap (Figure 2e). Whereas the distance between the two centers of the beam transmitted by the local metalens is significantly reduced due to the uniform demagnification (Figure 2e, blue), it remains unchanged when using the nonlocal metasurface (Figure 2e, red).

The image of the multiple Gaussians shown in Figure 2 is not just a proof-of-concept demonstration but is a realistic example that nicely models the imaging of fluorescent particles in biology, medical science, chemistry, etc. Interestingly, the sharpening of the spatial features not only applies to single or multiple Gaussians but also works for other patterns with a Gaussian line shape (as presented in the following section). Furthermore, although our simulations do not include other optical components, such as an objective lens, a nonlocal metasurface can be implemented in conventional optics to improve the resolution. Nonlocal metasurface-based imaging is diffraction-limited in that it cannot defeat the fundamental Abbe diffraction limit.[24] Nevertheless, for a given setup, the nonlocal metasurface can improve the setup resolution, originally determined by the numerical aperture of the system, by reducing the spot size or by sharpening the line width. See Section S4 (Supporting Information) for further details on the minimum resolvable distance. In addition, here we only present light localization, but selective magnification of the beam spots is also possible by encoding the OTF of a local concave lens (Section S5, Supporting Information).

2.3. Lithography Applications

The OTF of a nonlocal metasurface defined by the abovementioned method (Equation (3)) depends on the incidence parameters, such as the beam waist. Thus, it may result in distinct operations, i.e., the failure of the localization effect, under different incidences. Nevertheless, a nonlocal metasurface designed for a specific condition applies to other incidences with a smooth line shape to a certain level. For example, a nonlocal metasurface can sharpen patterned illumination with a Gaussian line shape. This makes it suitable for another promising application: photolithography. Implementing a nonlocal metasurface between the mask and photoresist sharpens the patterns and provides better resolution under the same conditions. To demonstrate this effect, a doughnut-shaped incidence periodically arranged in 3×3 pattern is considered (**Figure 3**a). The line shape of the ring is Gaussian with a half-line width of 75 μm (Figure 3d, black). When the incidence passes through the local metalens with $f = 1$ mm and propagates through the free space by 0.49f, all features, includ-

ing the distance between two neighboring rings, ring diameter, and line width, shrink by the same ratio of 0.56 (Figure 3b).

We imagine a nonlocal metasurface, the OTF of which is obtained by Equation (3) with different parameters: $w_0 = 75\mu$m and the cutoff of $6 \times 10^{-3} k_0$. Despite the difference between the **k** space profile of the single Gaussian and doughnut-shaped incidence, a localization effect is observed; only the line width is demagnified, whereas the distance between the rings and ring diameter barely changes (Figure 3c). This confirms the wide applicability of nonlocal metasurface for different incidences with smooth line shapes. The cross-sectional intensity profiles clearly show that the nonlocal metasurface selectively reduces the line width by a ratio of approximately 0.53 while retaining the spatial position of the patterns (Figure 3d). The discrepancy between the incidence used to determine the OTF and the doughnut-shaped incidence makes the localization ratio slightly different from the analytic value and also induces the four-fold rotational (C_4) pattern in Figure 3c. Moreover, the transmitted beam profiles can be converted into binary images by assuming a threshold value, above which the photoresist is polymerized. Binary images with a threshold of 0.3 (Figure 3e) demonstrate the successful line width reduction using the nonlocal metasurface. Note that the line width of the binary patterns depends on the threshold and can be changed by setting a different value.

2.4. Proposal of a Realistic Nonlocal Metasurface

As a proof-of-concept, we suggest a nonlocal metasurface consisting of a perforated high-index dielectric layer, a low-index dielectric layer, and another high-index dielectric layer, from top to bottom, on a silicon dioxide (SiO_2) substrate as a 2D analog light localizer working under unpolarized light (**Figure 4a**). The air hole in the top layer is periodically arranged in a square lattice and functions as a high-contrast grating. This trilayer design is adapted from previous studies on space compression and image differentiation by Guo et. al.[18,25] for its strong nonlocality originating from the guided-mode resonance. Considering the conceptual nature of the previously reported design, which is not experimentally feasible due to the requirement of a lossless high-index material and structures being freestanding and floating in air, we propose an alternative design using readily available materials, hydrogenated amorphous silicon (a-Si:H) as the high-index dielectric and SiO_2 as the low-index dielectric. The refractive indices of a-Si:H and SiO_2 are $3.5 + 0.046i$ and 1.457, respectively.[26,27] The five geometric parameters, lattice constant a, radius of the air hole r, upper a-Si:H thickness t_1, SiO_2 thickness t_2, and bottom a-Si:H thickness t_3, are obtained using particle swarm optimization by setting the localization ratio as the cost function to be minimized. Because of the significant dependence of the localization ratio on the lattice constant (Section S8, Supporting Information), the inertia weight in the optimization is set as zero. The optimized geometric parameters for operation at $\lambda = 632.8$ nm and $w_0 = 100\mu$m are as follows: $a = 438$ nm, $r = 194$ nm, $t_1 = 171$ nm, $t_2 = 1492$ nm, and $t_3 = 151$ nm.

For light incident from the air, the OTF of this nonlocal metasurface has strong polarization- and incident-angle-sensitive characteristics, which are common features of the guided-mode resonance[28–32] (Figure 4b). Under normal incidence, the incident light couples with the evanescent channel in the SiO_2 slab via diffraction and propagates laterally, guided by adjacent high-index layers. When the incidence is obliquely injected, this in-plane guided mode is maintained under p polarization at a sufficiently small incident angle ($\lesssim 5°$) but breaks down rapidly under s polarization where diffraction does not occur, leading to polarization- and incident-angle-selective behaviors within a narrow **k** regime ($|\mathbf{k}| \leq 0.01 k_0$) (see Section S6, Supporting Information for details).

The major cause of light localization in this metasurface is the low OTF at $\mathbf{k} = 0$, which suppresses the relative strength of the zero-spatial-frequency component, thereby broadening the overall **k** space profile. Without satisfying this requirement, analog light localization cannot be achieved because the transmitted beam is a superposition of the original beam and higher-order terms, which are insufficient to alter the overall beam shape (Section S2, Supporting Information). Another noticeable feature of the OTF is that $|t_s|$ exhibits a diverging amplitude along the k_x- and k_y-axes at small **k**, whereas $|t_p|$ maintains a low amplitude. These distinct behaviors result in the compression of the incident light spot when combined, as follows: The **k** space profile of the incidence is decomposed into s and p polarizations and then multiplied by the 2×2 OTF matrix (see the Experimental Section for details). For an incidence polarized along the horizontal (x-axis) direction, the p-polarized component of the transmitted beam has an elliptical beam shape similar to that of the incidence but has a slightly elongated feature along the vertical direction. In contrast, the s-polarized component has two vertically aligned, strong hotspot-like beam shapes at approximately $y = \pm 1.05 w_0$ due to the increasing amplitude. Importantly, the p- and s-polarized components have opposite phases at the hotspots, thereby leading to destructive interference that reduces the overall spot size, particularly along the y-axis. This corresponds to 1D light localization. Similar but a 90°-rotated feature is observed under vertical polarization because of the C_4 symmetry of the structure. The details can be found in the Section S7 (Supporting Information).

The superposition of the two results in a beam with a smaller spot size along both horizontal and vertical directions under unpolarized incidence, indicating the realization of 2D analog light localization (Figure 4c,d). The OTF (Figure 4b) not ideal as that shown in Figure 1d gives rise to sidelobes. The sidelobes are C_4 symmetric originally but have a slightly tilted pattern due to the nonzero cross-polarized components. The cross-sectional intensity profiles show that the localization ratio is approximately 0.74 and the sidelobe intensity is less than $1/e^2$. Because of the guided-mode resonance, the OTF and consequently the light localization effect depend strongly on the lattice constant. Such strong dependence is a common characteristic found in similar designs.[18,25] This allows us to design nonlocal metasurfaces with the desired localization ratio and sidelobe by fine-tuning the lattice constant (Section S8, Supporting Information). For easier experimental demonstration, searching for a metasurface design that is robust to changes in geometric parameters holds promise. In addition, a nonlocal metasurface can be designed for a smaller w_0 that reaches a few micrometers using the same principle, for example, by optimizing the geometric parameters to produce an OTF similar to those shown in Figure 4b in a wider **k** space range.

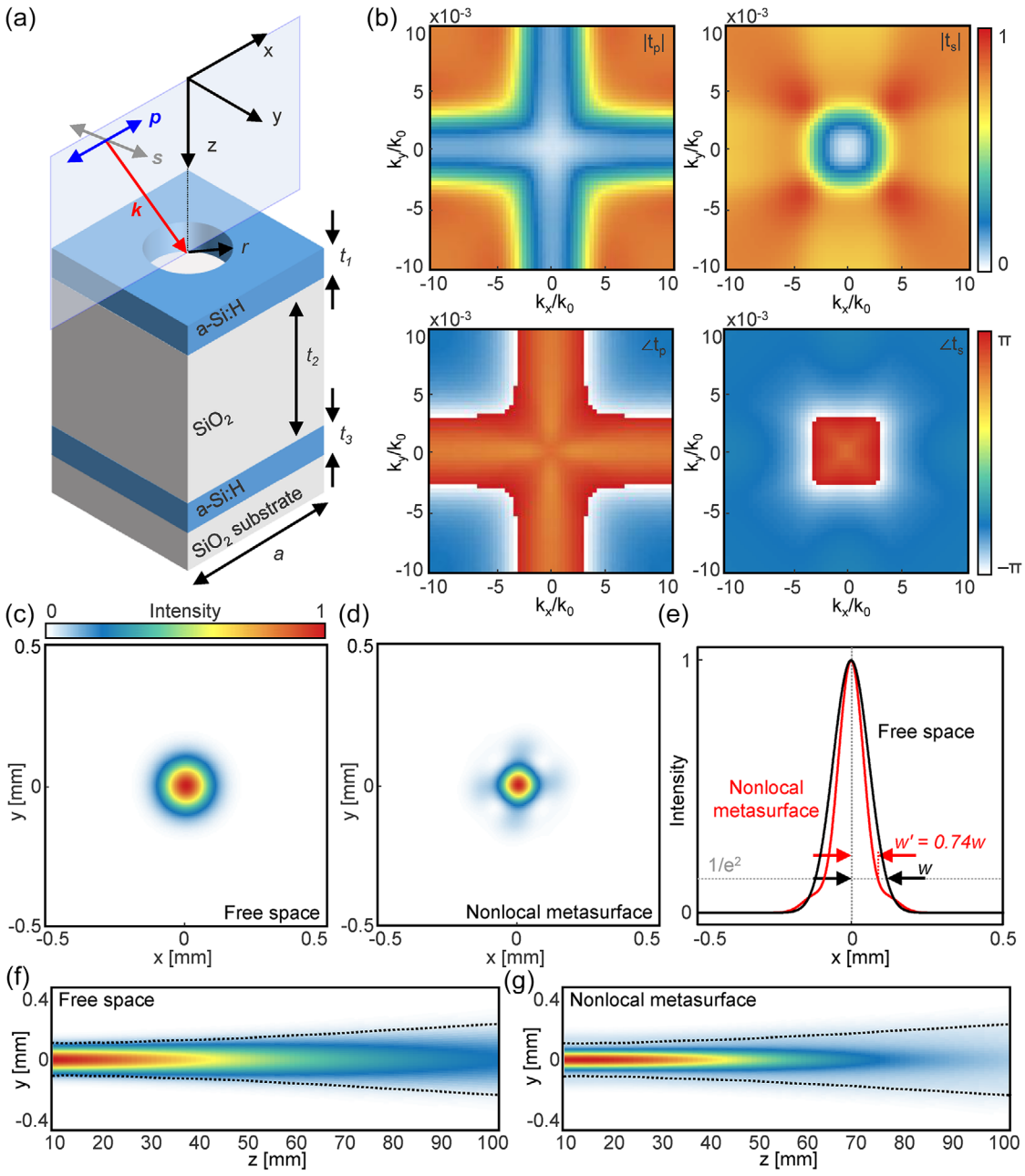

Figure 4. Realistic nonlocal metasurface for the light localization. a) Unit cell and b) OTF of the metasurface. c, d) Intensity profiles of beams propagated (c) without and (d) with the metasurface when the incidence is an unpolarized single Gaussian beam and $z_p = 30$ mm. e) Cross-sectional intensity profiles along the *x*-axis. f, g) Intensity profiles in the *yz* plane (f) without and (g) with the metasurface. Black curves indicate the beam waist of the Gaussian beam in the free space.

For completeness, Figure 4f,g present the evolution of the intensity profile with and without the metasurface during the free space propagation. Note that the metasurface and Gaussian focus of the incidence lie at $z = 0$. A Gaussian beam propagating in free space without passing through the metasurface follows a Gaussian beam expression and exhibits a diverging beam radius that obeys $w(z) = w_0\sqrt{1+F^2}$, where $F = z/z_R$ is the propagation factor (Figure 4f). In contrast, the simulation results of the beam propagating through the metasurface prove that the metasurface compresses the incidence not only at a specific propagation distance, but over a broad range (Figure 4g). Considering that the beam radius of the propagating Gaussian naturally enlarges (Figure 4g, black dashed), the central beam remains well localized even at a relatively far distance. However, compared to the center intensity, which decreases during propagation, the change in the sidelobe intensity is considerably less, leading to an increase in the relative strength of the sidelobe with increasing propagation distance (see Section S9, Supporting Information).

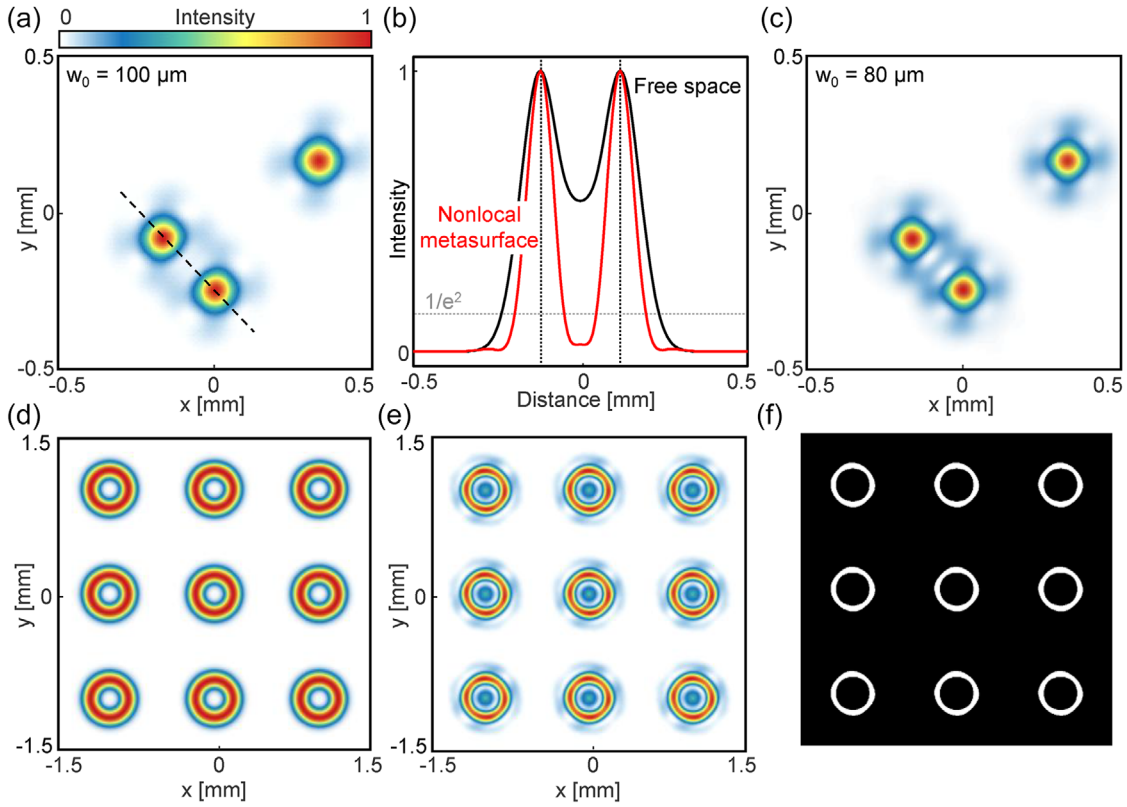

Figure 5. Imaging and lithography applications of the realistic nonlocal metasurface. a) Intensity profiles of the beam transmitted through the nonlocal metasurface when the incidence is the three Gaussian beams with $w_0 = 100\mu$m (Figure 2a). b) Cross-sectional intensity profiles along the black dashed line. c) Intensity profiles of the transmitted beam when $w_0 = 80\mu$m. d, e) Intensity profiles of the (d) incidence and (e) beam transmitted through the nonlocal metasurface when the half-line width of the doughnut-shaped beam is 100 μm. f) Binary image of (e) when the threshold is 0.5. $z_p = 30$ mm for imaging and 3 mm for lithography.

Finally, diffraction-limited imaging and lithography applications using a realistic nonlocal metasurface are demonstrated (**Figure 5**). Under triple Gaussian incidence shown in Figure 2a, the nonlocal metasurface selectively compresses the individual spots and retains their initial positions, as expected (Figure 5a). For two Gaussians placed nearby, the localized beam and sidelobe spatially overlap, generating unwanted noise, but their intensities are low compared with the spot intensity. Because of the localization effect, the two beams are more clearly distinguishable (Figure 5b). Although the nonlocal metasurface is optimized to operate for $w_0 = 100\mu$m, it also localizes a Gaussian with a different spot size $w_0 = 80\mu$m (Figure 5c, see also Section S10 and Figure S13, Supporting Information). Meanwhile, when the incidence has nonsmooth patterns, such as images with sharp edges, the metasurface supports 2D analog edge detection rather than light localization (Section S10 and Figure S14, Supporting Information). This is because a metasurface for edge detection has similar requirements: a vanishing OTF at the **k** space origin.[25,33–36] Therefore, although it has not been mentioned before, the previously proposed metasurface for 2D edge detection may provide light localization if the incidence changes from a binary, sharp image to a smooth one such as the Gaussian beam.[25] However, it does not imply that all metasurfaces for 2D edge detection provide such an effect, because most of their OTF do not change drastically in a narrow **k** regime. For instance, the single-layer metasurface for 2D edge detection[35] cannot reduce the light spot size for $w_0 = 100\mu$m (Section S11, Supporting Information).

We then examine the nonlocal metasurface under a periodically arranged doughnut-shaped incidence to prove its applicability to lithography (Figure 5d–f). Although this nonlocal metasurface is designed to localize a Gaussian beam, it successfully operates under patterned illumination with smooth line shape; the metasurface selectively reduces the line width of the incidence without altering any other features or compromising the overall pattern (Figure 5d,e). The distortion originating from the lack of rotational symmetry of the OTF is insignificant, especially at their binary patterns (Figure 5e,f). These results demonstrate that despite its incident-dependent characteristics, the nonlocal metasurface covers a wide range of incidences and thus is applicable to various circumstances.

3. Conclusion

A nonlocal metasurface that operates as a 2D analog light localizer is proposed and numerically demonstrated. Gaussian beams or patterned illumination with a Gaussian line shape are sharpened after propagating through the metasurface with an ideal OTF. To realize this 2D localization effect under unpolarized incidence, an experimentally feasible metasurface is suggested based

on a trilayer structure with periodically arranged air holes on the top layer. The nonlocal metasurface localizes multiple Gaussian incidences and sharpens ring patterns with Gaussian line shapes, confirming its applicability to diffraction-limited imaging and lithography. In comparison to local lenses, the nonlocal metasurface has the advantage of controlling the spot size and line width of individual features while preserving other spatial information intact. The nonlocal metasurface also has a limitation in that it does not perform well under incidences that significantly differ from the predefined one. Because of their complementary functionalities, combined use of the local lenses and nonlocal metasurfaces will create new possibilities in analog image processing. Finally, the experimental realization of the light localization and its implementation in biological, medical, and environmental science and other interdisciplinary area will be promising.

4. Experimental Section

The OTFs of the nonlocal metasurfaces were computed using the commercial software COMSOL Multiphysics. Bloch periodic boundary conditions were applied along two lateral boundaries and periodic ports with perfectly matched layer conditions were applied along the vertical boundaries. The full-wave simulations were conducted under oblique incidences by varying the incident angle and plane. The beam profile after the nonlocal metasurface was then obtained by first decomposing the incidence $\mathscr{F}(\psi_i(\mathbf{r})) = \tilde{\psi}_i(\mathbf{k}) = \left(\tilde{\psi}_{ip}(\mathbf{k})\ \tilde{\psi}_{is}(\mathbf{k})\right)^T$ in the $\mathbf{k}$ space and then applying $\psi_t(\mathbf{r}) = \mathscr{F}^{-1}[\tilde{T}_{nl}(\mathbf{k})\mathscr{F}(\psi_i(\mathbf{r}))]$ using a home-built code written in MATLAB where the OTF of the metasurface

$$\tilde{T}_{nl}(\mathbf{k}) = \begin{pmatrix} \tilde{T}^{pp}_{nl}(\mathbf{k}) & \tilde{T}^{ps}_{nl}(\mathbf{k}) \\ \tilde{T}^{sp}_{nl}(\mathbf{k}) & \tilde{T}^{ss}_{nl}(\mathbf{k}) \end{pmatrix} \tag{4}$$

is a 2 by 2 matrix. Small but nonzero off-diagonal elements (amplitude < 0.1) were not shown in this paper but were included in the calculation. The beam after propagating for a distance could be obtained by applying a scalar diffraction operation. The Rayleigh–Sommerfeld diffraction theory was used to calculate the results shown in Figures 3 and 5e; the Fresnel diffraction theory was used for the remaining.

Supporting Information

Supporting Information is available from the Wiley Online Library or from the author.

Acknowledgements

This work was financially supported by the National Research Foundation (NRF) grants (NRF-2022R1C1C2004662, RS-2023-00218908, NRF-2022R1F1A1065453, NRF-2022M3C1A3081312, NRF-2019R1A5A8080290) funded by the Ministry of Science and ICT (MSIT) of the Korean government, the Korea Evaluation Institute of Industrial Technology (KEIT) grant (No. 1415179744/20019169, Alchemist project) funded by the Ministry of Trade, Industry and Energy (MOTIE) of the Korean government, the POSCO-POSTECH-RIST Convergence Research Center program funded by POSCO, and the POSTECH-Samsung Semiconductor Research Center (IO201215-08187-01) funded by Samsung Electronics.

Conflict of Interest

The authors declare no conflict of interest.

Data Availability Statement

The data that support the findings of this study are available from the corresponding author upon reasonable request.

Keywords

compression, guided-mode resonance, nonlocality, photonic crystal, squeeze

Received: July 30, 2023
Revised: February 7, 2024
Published online: March 12, 2024

[1] M. Born, E. Wolf, *Principles of optics*, Cambridge University Press, Cambridge **2013**.
[2] N. Yu, P. Genevet, M. A. Kats, F. Aieta, J.-P. Tetienne, F. Capasso, Z. Gaburro, *Science* **2011**, *334*, 333.
[3] W. T. Chen, A. Y. Zhu, V. Sanjeev, M. Khorasaninejad, Z. Shi, E. Lee, F. Capasso, *Nat. Nanotechnol.* **2018**, *13*, 220.
[4] S. Wang, P. C. Wu, V.-C. Su, Y.-C. Lai, M.-K. Chen, H. Y. Kuo, B. H. Chen, Y. H. Chen, T.-T. Huang, J.-H. Wang, R.-M. Lin, C.-H. Kuan, T. Li, Z. Wang, S. Zhu, D. P. Tsai, *Nat. Nanotechnol.* **2018**, *13*, 227.
[5] R. Paniagua-Dominguez, Y. F. Yu, E. Khaidarov, S. Choi, V. Leong, R. M. Bakker, X. Liang, Y. H. Fu, V. Valuckas, L. A. Krivitsky, A. I. Kuznetsov, *Nano Lett.* **2018**, *18*, 2124.
[6] G. Yoon, K. Kim, D. Huh, H. Lee, J. Rho, *Nat. Commun.* **2020**, *11*, 2268.
[7] G. Yoon, K. Kim, S.-U. Kim, S. Han, H. Lee, J. Rho, *ACS Nano* **2021**, *15*, 698.
[8] M. Pan, Y. Fu, M. Zheng, H. Chen, Y. Zang, H. Duan, Q. Li, M. Qiu, Y. Hu, *Light Sci. Appl.* **2022**, *11*, 195.
[9] J. Rho, *MRS Bull.* **2020**, *45*, 180.
[10] J. Kim, J. Seong, W. Kim, G.-Y. Lee, S. Kim, H. Kim, S.-W. Moon, D. K. Oh, Y. Yang, J. Park, J. Jang, Y. Kim, M. Jeong, C. Park, H. Choi, G. Jeon, K.-i. Lee, D. H. Yoon, N. Park, B. Lee, H. Lee, J. Rho, *Nat. Mater.* **2023**, *22*, 474.
[11] T. Badloe, Y. Kim, J. Kim, H. Park, A. Barulin, Y. N. Diep, H. Cho, W.-S. Kim, Y.-K. Kim, I. Kim, J. Rho, *ACS Nano* **2023**, *17*, 14678.
[12] D. Jeon, K. Shin, S.-W. Moon, J. Rho, *Nano Converg.* **2023**, *10*, 1.
[13] S. So, J. Mun, J. Park, J. Rho, *Adv. Mater.* **2023**, *35*, 2206399.
[14] A. Overvig, A. Alú, *Laser Photonics Rev.* **2022**, *16*, 2100633.
[15] K. Shastri, F. Monticone, *Nat. Photon.* **2023**, *17*, 36.
[16] E. Noether, *Transp. Theory Stat. Phys.* **1971**, *1*, 186.
[17] J. W. Goodman, *Introduction to Fourier optics*, Roberts and Company publishers, Greenwood Village, CO **2005**.
[18] C. Guo, H. Wang, S. Fan, *Optica* **2020**, *7*, 1133.
[19] O. Reshef, M. P. DelMastro, K. K. Bearne, A. H. Alhulaymi, L. Giner, R. W. Boyd, J. S. Lundeen, *Nat. Commun.* **2021**, *12*, 3512.
[20] O. Y. Long, C. Guo, W. Jin, S. Fan, *Phys. Rev. Appl.* **2022**, *17*, 024029.
[21] K. Shastri, O. Reshef, R. W. Boyd, J. S. Lundeen, F. Monticone, *Optica* **2022**, *9*, 738.
[22] A. Chen, F. Monticone, *ACS Photon.* **2021**, *8*, 1439.
[23] M. Mrnka, E. Hendry, J. Láčík, R. A. Lennon, L. E. Barr, I. R. Hooper, D. B. Phillips, *arXiv preprint arXiv:2110.15022*, **2021**.
[24] E. Abbe, *Arch. Microsc. Anat.* **1873**, *9*, 413.
[25] C. Guo, M. Xiao, M. Minkov, Y. Shi, S. Fan, *Optica* **2018**, *5*, 251.
[26] Y. Yang, G. Yoon, S. Park, S. D. Namgung, T. Badloe, K. T. Nam, J. Rho, *Adv. Mat.* **2021**, *33*, 2005893.
[27] I. H. Malitson, *J. Opt. Soc. Am.* **1965**, *55*, 1205.

[28] S. S. Wang, R. Magnusson, *Appl. Opt.* **1993**, *32*, 2606.
[29] A. Hessel, A. A. Oliner, *Appl. Opt.* **1965**, *4*, 1275.
[30] G. Quaranta, G. Basset, O. J. F. Martin, B. Gallinet, *Laser Photonics Rev.* **2018**, *12*, 1800017.
[31] J. Jang, T. Badloe, Y. Yang, T. Lee, J. Mun, J. Rho, *ACS Nano* **2020**, *14*, 15317.
[32] L. Huang, R. Jin, C. Zhou, G. Li, L. Xu, A. Overvig, F. Deng, X. Chen, W. Lu, A. Alù, A. E. Miroshnichenko, *Nat. Commun.* **2023**, *14*, 3433.
[33] J. Zhou, H. Qian, J. Zhao, M. Tang, Q. Wu, M. Lei, H. Luo, S. Wen, S. Chen, Z. Liu, *Nat. Sci. Rev.* **2020**, *8*, nwaa176.
[34] A. Komar, R. A. Aoni, L. Xu, M. Rahmani, A. E. Miroshnichenko, D. N. Neshev, *ACS Photon.* **2021**, *8*, 864.
[35] Y. Zhou, H. Zheng, I. I. Kravchenko, J. Valentine, *Nat. Photon.* **2020**, *14*, 316.
[36] A. Cordaro, H. Kwon, D. Sounas, A. F. Koenderink, A. Alù, A. Polman, *Nano Lett.* **2019**, *19*, 8418.